

Songbird Ventral Pallidum Sends Diverse Performance Error Signals to Dopaminergic Midbrain

Highlights

- Songbird ventral pallidum (VP) is required for song learning
- VP neurons encode song performance error and precise song timing
- VP sends error and error prediction signals to dopaminergic midbrain
- VP receives input from auditory areas and the vocal motor song system

Authors

Ruidong Chen, Pavel A. Puzerey,
Andrea C. Roeser, ..., Kamal Maher,
Alexander R. Farhang,
Jesse H. Goldberg

Correspondence

jessehgoldberg@gmail.com

In Brief

Songbird dopamine neurons encode error signals important for learning. Chen et al. discover that the ventral pallidum is required for song learning, encodes syllable timing, and sends error and error prediction signals to dopaminergic midbrain.



Songbird Ventral Pallidum Sends Diverse Performance Error Signals to Dopaminergic Midbrain

Ruidong Chen,¹ Pavel A. Puzerey,¹ Andrea C. Roeser,¹ Tori E. Riccelli,¹ Archana Podury,¹ Kamal Maher,¹ Alexander R. Farhang,¹ and Jesse H. Goldberg^{1,2,*}

¹Department of Neurobiology and Behavior, Cornell University, Ithaca, NY 14853, USA

²Lead Contact

*Correspondence: jessehgoldsberg@gmail.com

<https://doi.org/10.1016/j.neuron.2019.04.038>

SUMMARY

Motor skills improve with practice, requiring outcomes to be evaluated against ever-changing performance benchmarks, yet it remains unclear how performance error signals are computed. Here, we show that the songbird ventral pallidum (VP) is required for song learning and sends diverse song timing and performance error signals to the ventral tegmental area (VTA). Viral tracing revealed inputs to VP from auditory and vocal motor thalamus, auditory and vocal motor cortex, and VTA. Our findings show that VP circuits, commonly associated with hedonic functions, signal performance error during motor sequence learning.

INTRODUCTION

When practicing a piano concerto, you could evaluate your performance relative to a fixed template, such as an auditory memory of Glenn Gould playing Chopin's Prelude No. 4, yet reinforcement learning (RL) theory suggests improved learning if you instead learn from prediction errors, in which a note is reinforced only if it sounds better (closer to the template) than predicted based on your past performance (Sutton and Barto, 1998). RL proceeds via incremental improvement in performance quality, requiring performance to be evaluated against benchmarks that change with practice (Schmidt et al., 2018; Thelen, 1995). Neural mechanisms of performance benchmarking and evaluation remain poorly understood.

Songbirds provide a tractable model system to study performance evaluation. First, songbirds have a specialized circuit, the "song system," that includes a projection from ventral tegmental area (VTA) dopamine (DA) neurons to the striatopallidal nucleus area X (Gale et al., 2008; Reiner et al., 2004). Second, zebra finches gradually learn to imitate a sequence of song notes, or syllables, acquired from a single tutor, suggesting they have a "fixed template" they aspire to learn (Marler, 1997). Yet, consistent with RL theory, song syllables are not evaluated exclusively against this fixed template but are additionally evaluated against syllable-specific performance

benchmarks that change with practice. Specifically, area-X-projecting VTA (VTA_X) DA neurons are phasically suppressed by distorted auditory feedback (DAF) during singing (Gadagkar et al., 2016). DAF, though not generally aversive (Murdoch et al., 2018), induces a perceived vocal error on distorted renditions such that undistorted renditions are reinforced (Ali et al., 2013; Andalman and Fee, 2009; Hamaguchi et al., 2014; Keller and Hahnloser, 2009; Turner and Brainard, 2007). Over day timescales, DAF also reduces the predicted quality (i.e., proximity to template) of DAF-targeted syllables. When a reliably distorted target syllable is left undistorted, VTA_X neurons exhibit phasic bursts at the precise moment of the song when DAF is predicted to occur but does not occur, and the magnitude of this burst depends on past error probability (Gadagkar et al., 2016). Thus, VTA_X neurons signal errors in predicted song quality, i.e., the difference between how good (close to the template) a syllable sounded and how good it was predicted to be based on recent practice.

To signal performance prediction error, songbird DA neurons must compute the difference between actual "just heard" error and the error that was predicted at that specific time step of the song. The roles of upstream projections to VTA in these computations remain unclear. One projection to VTA comes from a high-order auditory cortical area that forms a "cup" around the robust vocal motor nucleus of the arcopallium (RAcup) (Bottjer et al., 2000; Kelley and Nottebohm, 1979; Mello et al., 1998; Vates et al., 1996). RAcup, which is located in the ventral intermediate arcopallium (AIV), is necessary for song learning and sends error signals to VTA (Gale et al., 2008; Mandelblat-Cerf et al., 2014), but it remains unknown how AIV influences VTA firing.

The second major forebrain input to VTA in songbirds comes from a ventral pallidal (VP) region outside the classic song system, ventral and medial to area X (Gale and Perkel, 2010; Gale et al., 2008), yet it remains unknown if VP is important for song learning and what, if any, singing-related signals it exhibits.

Here, we combine lesion, electrophysiology, and viral tracing studies to demonstrate for the first time that songbird VP is required for learning, exhibits performance error signals, and receives previously unknown inputs from nuclei of the "classic" song system. More generally, our results directly implicate VP in learning a purely motor sequence task like birdsong.



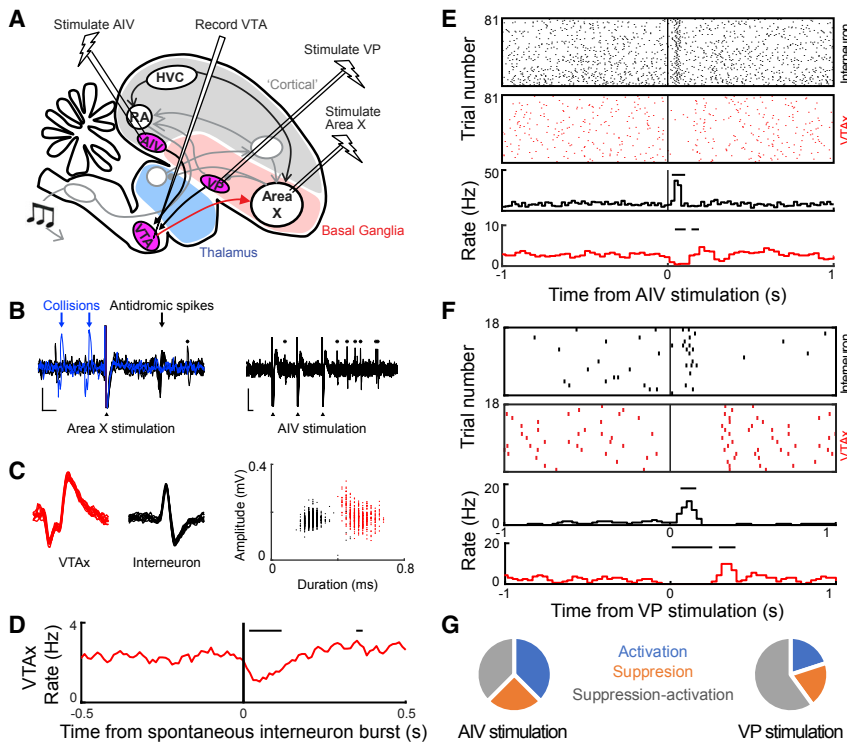


Figure 1. Auditory Cortical and VP Stimulation Drive Diverse Changes in VTA_x Neuron Firing

(A) Schematic of the experimental strategy used to record VTA_x neuronal responses to AIV and VP stimulation. (B–G) Experiment conducted on simultaneously recorded wide-spiking VTA_x neurons and thin-spiking VTA interneurons. (B) Antidromic identification (left), and AIV stimulation (right). Arrows show VTA_x antidromic spiking (black) and collisions (blue), asterisks indicate interneuron spikes, and filled triangles represent stimulation artifacts. Scale bars represent 0.1 mV (vertical) and 2 ms (horizontal). (C) Left: overlay of raw trace from 10 VTA_x spikes (red). Middle: 10 VTA interneuron spikes (black). Right: amplitude and duration of all recorded VTA_x (red) and interneuron (black) spikes. (D) Cross-correlogram of spontaneous firing between the two units. Horizontal bars indicate a significant response ($p < 0.05$, Z test) (STAR Methods). (E) Raster plots (top) and rate histograms (bottom) of interneuron (black) and VTA_x neuron (red), aligned to AIV stimulation. Horizontal bars indicate a significant response ($p < 0.05$, Z test) (STAR Methods). (F) Same as (E) for VP stimulation. (G) Summary of VTA_x response types ($n = 8$ neurons with AIV stimulation, $n = 5$ neurons with VP stimulation).

See also Figures S1 and S2.

RESULTS

Auditory Cortical Stimulation Causes Diverse Responses in VTA_x Neurons

To identify circuits important for performance evaluation, we injected retrograde tracer into the area-X-projecting part of VTA, where performance error encoding DA neurons important for song learning reside (Gadagkar et al., 2016; Hisey et al., 2018; Hoffmann et al., 2016; Xiao et al., 2018). Consistent with past work, retrogradely labeled neurons were observed in AIV (Bottjer et al., 2000; Gale et al., 2008; Kelley and Nottebohm, 1979; Mandelblat-Cerf et al., 2014; Mello et al., 1998; Vates et al., 1996; Figures S1A and S1B). Previous studies showed that during singing, DAF causes activation of VTA-projecting AIV neurons and, at a slightly longer latency, pauses in VTA_x neurons (Gadagkar et al., 2016; Mandelblat-Cerf et al., 2014).

To test if AIV stimulation affects VTA_x firing, we recorded VTA neurons while electrically stimulating AIV in anesthetized birds ($n = 7$ birds; Figure 1A). AIV stimulation induced phasic rate changes in all wide-spiking, antidromically identified VTA_x neurons ($n = 8$ antidromic neurons, spike width 0.38 ± 0.03 ms; Figures S2K and S2L; Schultz and Romo, 1987). Responses included suppression followed by activation ($n = 3$; Figures S2B–S2D; latency 75 ± 19 ms), activations ($n = 3$; Figures S2H, and S2I; latency 112 ± 54 ms), and suppressions ($n = 2$; Figures 1F and S2E, and S2J; latency $15\text{--}35$ ms). In putative VTA interneurons with thin spikes ($n = 13$, spike width 0.26 ± 0.02 ms; STAR Methods), AIV stimulation caused low-latency activations ($n = 7$, latency 29 ± 12 ms) or suppressions ($n = 5$, latency 20 ± 7.8 ms). When we recorded simultaneously from a VTA_x neuron

and a thin spiking interneuron at the end of the same electrode, we found that AIV stimulation activated the interneuron, which in turn could suppress the VTA_x neuron (Figures 1B–1F).

Together, these findings suggest that VTA contains complex local circuitry, including one that implements feedforward inhibition to invert excitatory signals from AIV, consistent with the idea that performance-error-induced activations in AIV can drive pauses in VTA_x firing during singing. Notably, the AIV-VTA projection resembles cortical projections to VTA in mammals that also can target local GABAergic interneurons and inhibit dopaminergic firing (Beier et al., 2015; Carr and Sesack, 1999; Creed et al., 2014; Moreines et al., 2017; Patton et al., 2013).

VP Stimulation Causes Diverse Responses in VTA_x Neurons

Following tracer injection into the VTA_x, retrogradely labeled neurons were also observed in a ventromedial basal ganglia region termed VP in previous studies (Figure S1C; Gale and Perkel, 2010; Gale et al., 2008; Reiner et al., 2004). To test if VP can influence VTA_x activity, we electrically stimulated VP while recording antidromically identified VTA_x neurons in anesthetized birds ($n = 4$ birds; Figure 1A). Response to VP stimulation included suppression followed by activation ($n = 3/5$ neurons tested; Figures 1G and S2N–S2P), suppression ($n = 1/5$; Figure S2Q), and activation ($n = 1/5$; Figure S2R). Responses to VP stimulation had lower latency than those to AIV (VP: 15 ± 2.7 ms, AIV: 22.8 ± 7.8 ms, $p < 0.01$, Wilcoxon signed-rank [WRS] test; Figure S2L). The observation that VP can influence VTA_x activity in complex ways is consistent with diverse

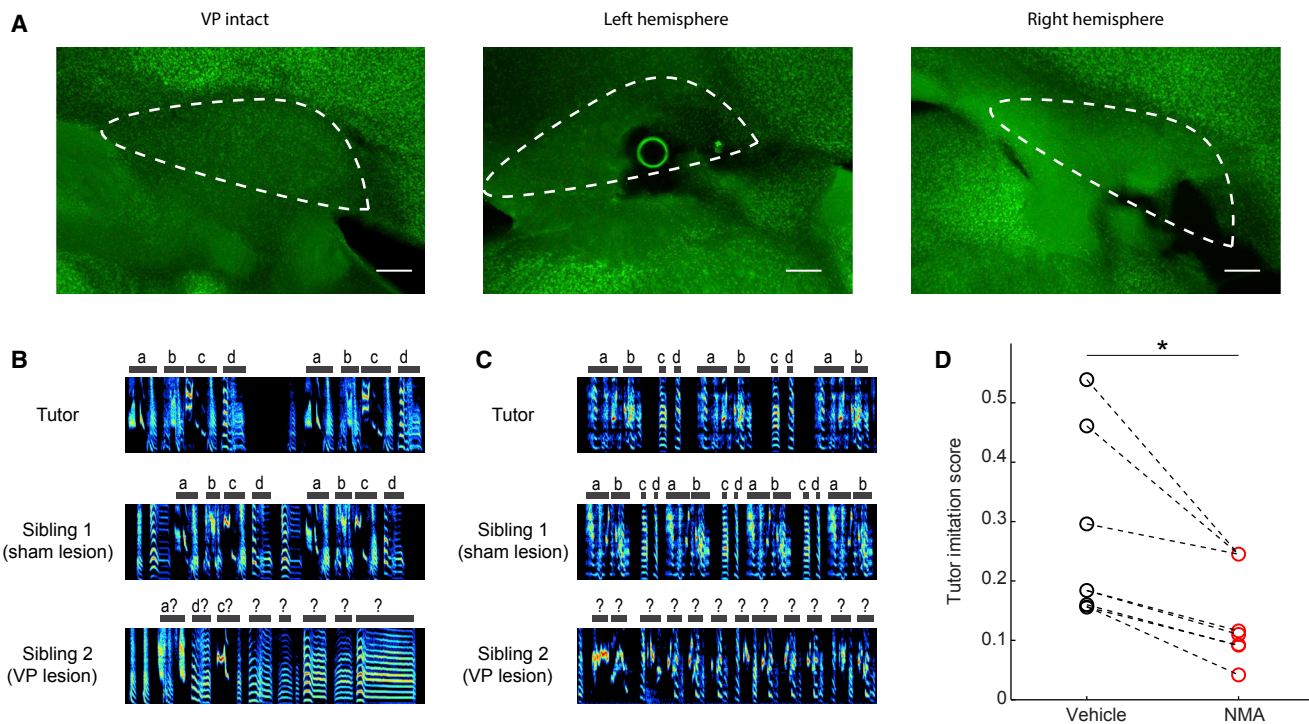


Figure 2. VP Lesions Impair Song Learning

(A) Lesions were confirmed in neuronal nuclear stained (anti-NeuN) slices as extensive cell death. Scale bars, 200 μ m.
 (B) Tutor song (top), adult song of sham-lesioned (middle), and VP-lesioned (bottom) siblings. Each spectrogram is 2 s long.
 (C) Same as (B) for another pair.
 (D) Adult song of VP-lesioned birds had lower similarity to their tutor compared to controls (rank-sum test between all controls and all lesioned birds, $p = 0.014$.
 $n = 7$ sham lesion, $n = 6$ VP lesion).

VTA-projecting cell types in VP (Person et al., 2008), as well as the presence of feedforward inhibition in VTA that can invert incoming signals.

VP Lesions Impair Song Learning

To test if VP is important for song learning, we conducted lesion experiments in juvenile birds. To specifically lesion the part of VP that is part of the area X-VP-VTA-area X loop previously hypothesized to play a role in learning (Gale and Perkel, 2010), we carried out electrophysiologically guided excitotoxic VP lesions in juvenile birds and evaluated their adult songs (STAR Methods). During lesion surgery, stimulation electrodes were implanted into area X, and the boundaries of orthodromic stimulation-evoked responses were mapped with recording electrodes in VP. This mapping specified the locations of excitotoxin injections (STAR Methods). VP lesions significantly impaired song learning (song imitation score, WRS test, $p = 0.014$, $n = 6$ lesion birds and 7 controls; STAR Methods; Figure 2).

Firing Patterns of VP Neurons in Singing Birds

To test how VP may guide learning, we recorded VP neurons in singing birds. With some exceptions detailed below, neurons could not easily be categorized into distinct cell classes, because they exhibited a continuum of mean firing rates, spike widths, and discharge patterns (firing rate in singing: 43 ± 3.3 Hz; range, 0.38–

310 Hz; spike width: 0.25 ± 0.008 ms; range 0.05–0.59 ms; CV_{ISI} in singing: 1.10 ± 0.03 ; range, 0.4–2.9; $n = 162$ neurons; Figures S3A–S3G). This heterogeneity is consistent with the diverse striatal and pallidal cell types intermingled inside the songbird VP (Person et al., 2008).

Notably, neuronal discharge heterogeneity is also observed in mammalian VP, leading several studies to categorize neurons on the basis of their responses to primary rewards and cues that predict them (Ahrens et al., 2016; Ito and Doya, 2009; Ottenheimer et al., 2018; Richard et al., 2016, 2018; Smith et al., 2009; Tachibana and Hikosaka, 2012; Tindell et al., 2004). Below we will proceed similarly by categorizing neurons on the basis of their responses to song error and syllable timing.

VP Neurons Exhibit Performance and Prediction Error Signals during Singing

To specifically test the role of VP neurons in learning, we used syllable-targeted DAF to control perceived error during our recordings (Andalman and Fee, 2009; Turner and Brainard, 2007; STAR Methods). Beginning days prior to recordings, a specific “target” song syllable was either distorted with DAF or, on randomly interleaved renditions, left undistorted altogether (distortion rate at target syllable $48.0\% \pm 1.4\%$, mean \pm SEM, $n = 39$ birds). Days of pre-training with syllable-targeted DAF reduces the predicted quality of target syllables such that undistorted renditions are

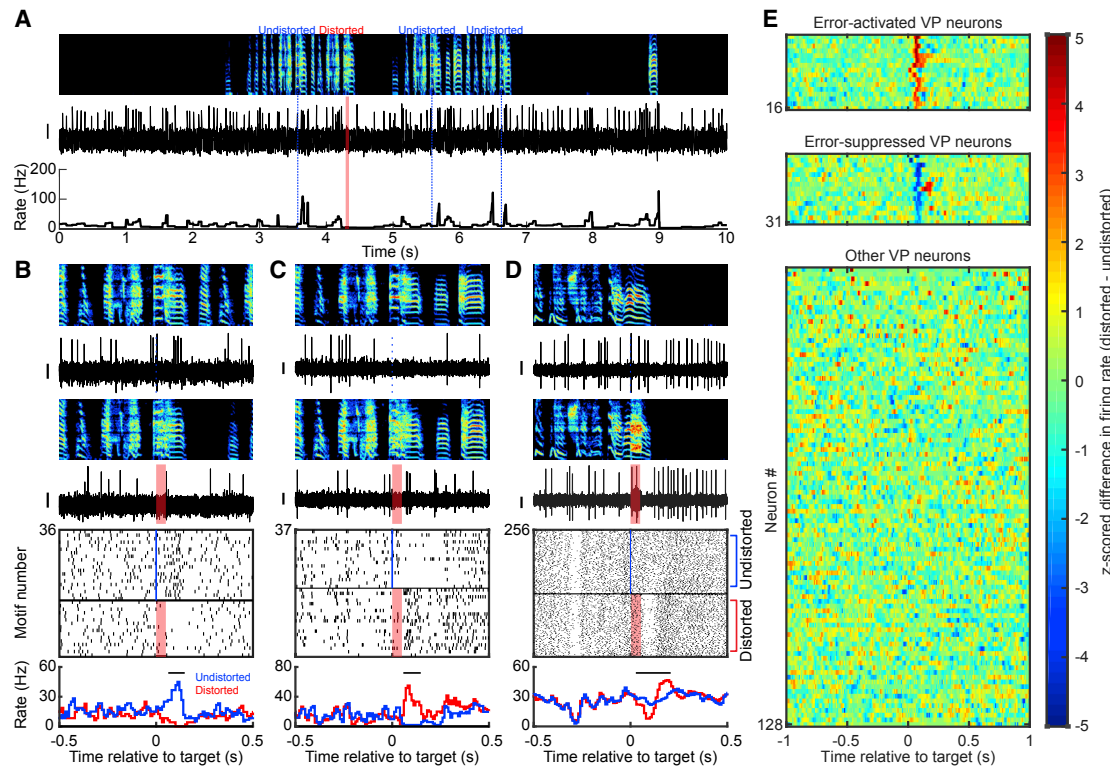


Figure 3. VP Neurons Exhibit Performance and Prediction Error Signals during Singing

(A) Spectrogram (top), spike discharge (middle), and instantaneous firing rate (bottom) of a prediction-error-encoding VP neuron (DAF, red shading; undistorted targets, blue lines).

(B) Expanded view of neuron from (A). Top to bottom: spectrograms, spiking activity during undistorted and distorted trials, corresponding spike raster plots, and rate histograms (all aligned to target onset). Horizontal bars in histograms indicate significant different responses to distorted and undistorted renditions, and a lack of horizontal bars indicates that no significant different response was detected (error response, $p < 0.05$, WRS test) (STAR Methods).

(C and D) Additional examples of error-activated (C) and error-suppressed (D) neurons (same format as B).

(E) Each row plots the Z-scored difference between distorted and undistorted target-aligned rate histograms. Error-activated neurons (top, $n = 16$), error-suppressed neurons (middle, $n = 15$), and non-error-responsive neurons (bottom, $n = 97$) are independently sorted by maximal Z score. Scale bar for spiking activity in (A)–(D) is 0.15 mV.

See also Figures S3–S5.

signaled as better than predicted by VTA_X DA neurons (Gadagkar et al., 2016).

To test if VP neurons exhibited online error responses, we compared the activity between randomly interleaved renditions of distorted and undistorted songs. We defined an error response as a significant difference of firing in distorted and undistorted renditions. Surprisingly, although there are no known inputs to VP that carry auditory information in awake singing birds, significant error responses were observed in 31/128 VP neurons tested (Figure 3) (assessed by WRS test on number of spikes in the 125-ms window following DAF onset time; Keller and Hahnloser, 2009; 34/162 neurons were not tested due to the low number of trials; STAR Methods). Neurons were either activated ($n = 16$) or suppressed ($n = 15$) by DAF during singing (quantified as Z-scored rate difference between undistorted and distorted renditions; STAR Methods). Biphasic responses were observed in 6/31 error-responsive neurons; initial suppressions (or activations) were followed by significant activations (or suppressions) (Figure 3D; STAR Methods).

A subset of error-responsive neurons exhibited a significant maximum or minimum of firing rate following undistorted, but not distorted, target times ($n = 10/31$ error-responsive neurons, $p < 0.05$, bootstrapping; STAR Methods). We term these “prediction error” responses, because they cannot be explained by the external DAF sound and occur only following better-than-predicted song outcomes (Gadagkar et al., 2016). Prediction error responses could be rate peaks ($n = 8$ error-suppressed neurons; Figure 3B) or nadirs ($n = 2$ error-activated neurons; Figure 3D).

Overall, the latencies and durations of error responses were similar to those observed in downstream VTA_X DA neurons (latency: 55.0 ± 3.8 ms; duration: 76.4 ± 7.0 ms; $n = 31$ cells; Figures S4A and S4B; STAR Methods).

To test if error responses were performance related (defined as error responses that only occur during singing) and not nonspecific auditory responses, we played back distorted and undistorted renditions of bird’s own song (BOS) to non-singing birds in a subset of recorded neurons. Auditory error responses were rarely observed following playback of distorted

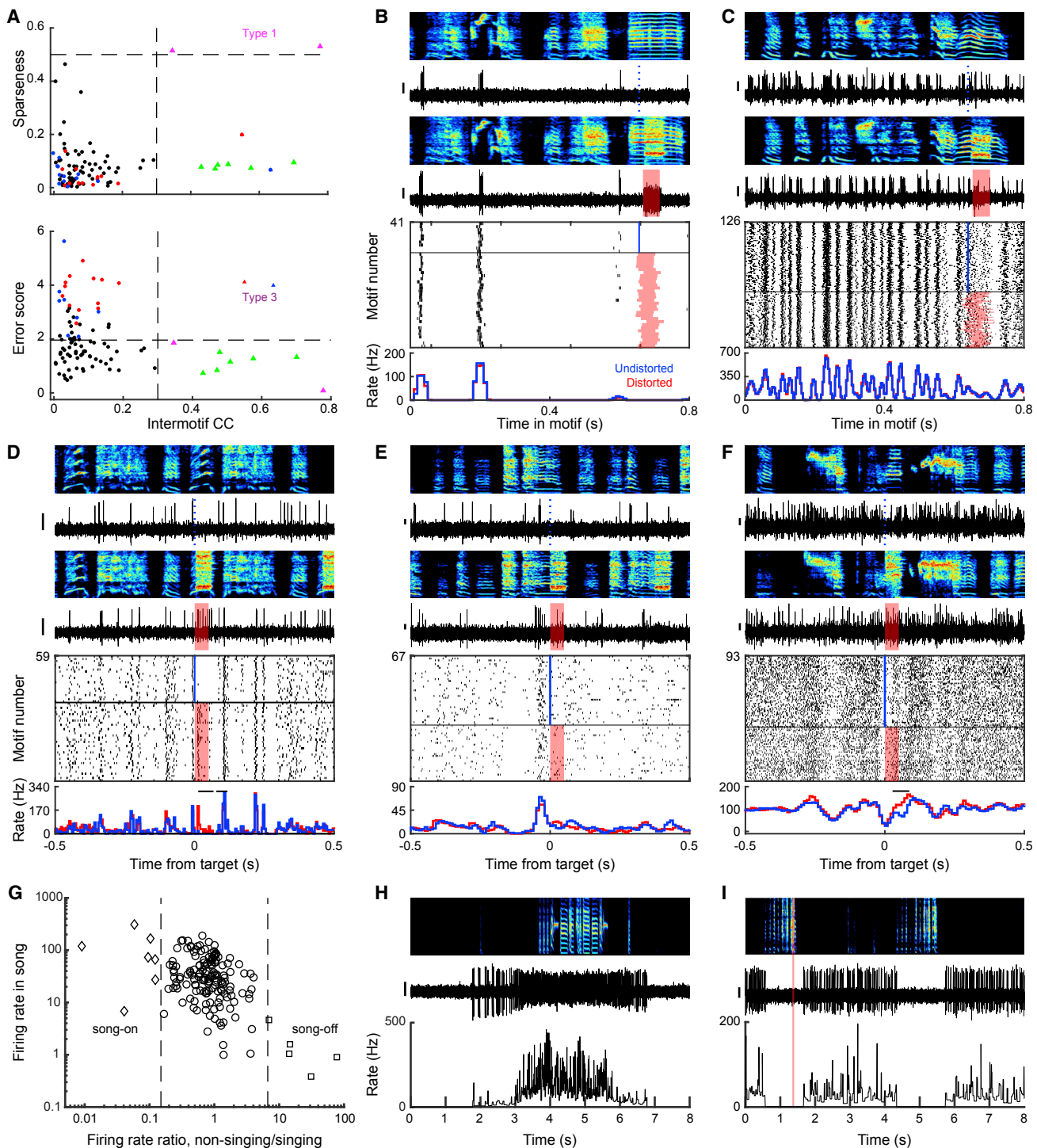


Figure 4. VP Neurons Exhibit Temporally Precise Song-Locked Activity during Singing

(A) Top: sparseness of song-locked VP neurons plotted against the inter-motif correlation coefficient (IMCC). Dashed lines: IMCC = 0.3 (vertical) and sparseness = 0.5 (horizontal). Bottom: maximum error score (absolute Z-scored difference between distorted and undistorted trials) plotted against IMCC. Dashed lines: IMCC = 0.3 and error score = 1.96.

(B–F) Top to bottom: spectrograms, spiking activity during undistorted and distorted trials, corresponding spike raster plots and rate histograms for a VP neuron with sparse, temporally precise discharge (B), one with time-locked bursts that tile the song (C), one with time-locked bursts and error response (D), one with significant rate maximum immediately before target time (E), and one with significant rate minimum at target time (F). Horizontal bars on top of rate histograms indicate a significant difference between distorted and undistorted firing ($p < 0.05$, WRS test).

(legend continued on next page)

versus undistorted BOS to awake, non-singing birds ($p > 0.05$ in 33/35 neurons tested, including 14/16 error-responsive neurons, WRS test) (Figures S5A–S5D). To test if error responses were attributable to different movement patterns following distortions, we used custom head-mounted accelerometers to quantify movement during recordings. Movement did not differ between distorted and undistorted renditions (Figure S5E), confirming that error responses were not attributable to body movement (Gadagkar et al., 2016). Together, these data demonstrate that VP neurons can exhibit error signals specifically during singing, consistent with performance error.

VP Neurons Exhibit Temporally Precise Song-Locked Activity during Singing

Many VP neurons also exhibited activity patterns temporally aligned to song. To quantify the precision of song-locked discharge, we calculated the pairwise inter-motif correlation coefficients (IMCCs) of instantaneous firing rates for all neurons recorded for 10 or more motifs (Goldberg et al., 2010; Goldberg and Fee, 2010; Kao et al., 2008; Olveczky et al., 2005; STAR Methods). A neuron that reliably discharges at the same time steps across song renditions will have an IMCC = 1; a neuron with random discharge unrelated to singing will have an IMCC = 0. Most VP neurons exhibited significant song-locked discharge with a precision that varied among the population ($p < 0.05$ in 96/162 neurons tested; IMCC = 0.13 ± 0.016 ; Figure 4A). Most neurons did not show time-locked responses to BOS playback ($p > 0.05$ in 33/35 neurons tested, including 21/23 song-locked neurons; STAR Methods).

Three cell “types” were distinguished by extremely precise song-locked firing (IMCC > 0.3) (Figure 4; $n = 10$). A first type exhibited ultra-sparse discharge aligned to specific song syllables ($n = 2$, sparseness index > 0.5; STAR Methods; Figures 4A and 4B). These sparse neurons’ discharge resembled striatal medium spiny neurons (MSNs) previously recorded in area X (Goldberg and Fee, 2010; Woolley et al., 2014) and support the previous finding that striatal and pallidal cell types can be intermingled in songbird VP (Person et al., 2008). A second type exhibited stereotyped, rhythmic firing patterns visible as high-frequency bursts aligned to specific song time steps with millisecond precision (Figures 4A and 4C; $n = 6$). In contrast to the first two types, which did not exhibit error responses, a third type exhibited error responses as well as time-locked response to BOS playback, consistent with a neuron that receives strong auditory input ($n = 2$, IMCC > 0.3 during BOS playback; Figures 4D, S5C, and S5D).

Most song-locked neurons also exhibited significant rate modulations at various time steps of the song ($n = 93/96$ with significant rate maximum or minimum; STAR Methods; Figures 4E and 4F). Finally, other neurons were distinguished by dramatic increase or decrease in firing rate at the transition between non-singing and singing states (Figures 4G–4I; $n = 12$, rate differ-

ence >85%). All of these diverse cell types were spatially intermingled (Figure S3H).

VP Sends Diverse Error- and Prediction-Related Signals to VTA

To test which VP signals are sent to VTA, we used antidromic and collision testing methods to identify VTA-projecting VP (VP_{VTA} , $n = 10$; Figures 5A and 5B) and putative non-VTA-projecting (VP_{Other} , $n = 92$) neurons ($n = 60$ not tested). Like the VP population more generally, VP_{VTA} neurons exhibited a range of firing rates and discharge patterns (Figure S3). However, VP_{VTA} neurons were significantly more likely to exhibit error responses than non-projectors ($n = 5/10$ VP_{VTA} neurons, 16/92 VP_{Other} neurons, $p < 0.05$, WRS test; STAR Methods).

VP_{VTA} neurons were also significantly more likely to exhibit a minimum in firing rate immediately prior to the target time in the song ($n = 5/10$ VP_{VTA} neurons, 12/92 VP_{Other} neurons, $p < 0.01$, WRS test; STAR Methods). These pre-target pauses are consistent with a predicted quality signal. One VP_{VTA} neuron exhibited a robust pre-target burst, but such pre-target activations were not enriched in the VP_{VTA} neurons relative to VP_{Other} neurons ($p > 0.05$, WRS test; STAR Methods). Together, these findings show that VP sends diverse error- and prediction-related signals to VTA.

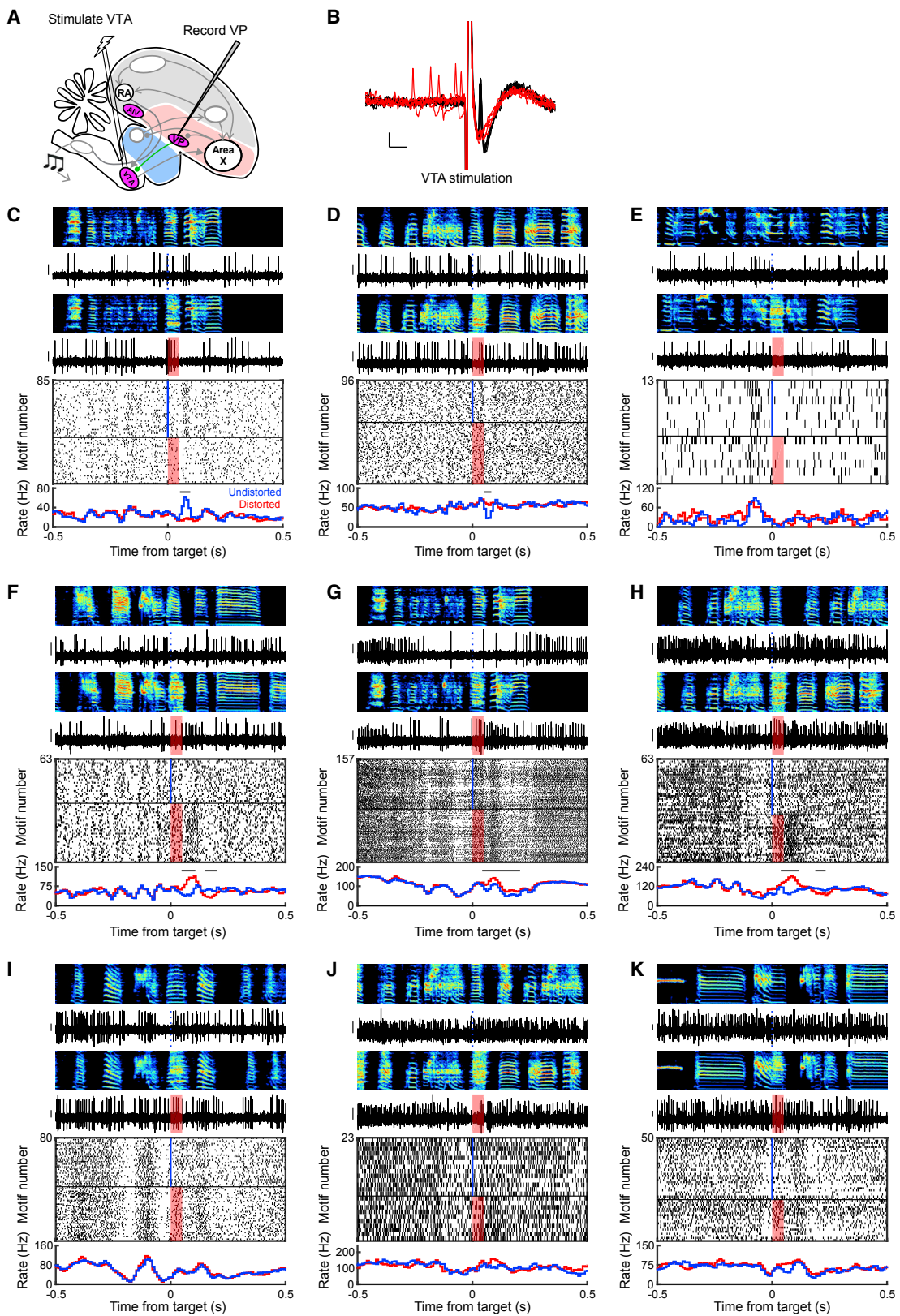
Viral Tracing Identifies Inputs to VP from Dopaminergic, Vocal Motor, and Auditory Regions

To test what inputs to VP could account for this diversity of singing and error-related firing, we combined retrograde and anterograde viral tracing strategies. Abundant fiber tracts course through VP, complicating the interpretation of results obtained with dextran and cholera toxin (CTB) tracers, which can be taken up by fibers of passage. We thus used a sparse GFP-expressing retrograde virus, self-complementary AAV9 (scAAV9-CBh-GFP), that is taken up by axon terminals (Xiao et al., 2018; STAR Methods). Following injection of viral tracer into VP, retrogradely labeled neurons were observed in several singing-related cortical, thalamic, and midbrain structures, including (1) robust nucleus of the arcopallium (RA), a vocal motor cortex-like nucleus known to send precise motor command signals to brainstem motor neurons (Leonardo and Fee, 2005; Sober et al., 2008; Yu and Margoliash, 1996; Figures S6A and S6B; retrograde labeling observed in 4/11 hemispheres); (2) uva, a motor thalamic nucleus known to send precise song timing information to HVC (5/19 hemispheres; Figures S6E–S6G) (Danish et al., 2017; Hamaguchi et al., 2016); (3) medial portion of the dorsolateral thalamus (DLM), the area-X-recipient thalamic nucleus known to send premotor signals to cortical lateral magnocellular nucleus of the anterior nidopallium (LMAN; 3/12 hemispheres; Figures S6M–S6O; Goldberg and Fee, 2012); (4) AIV, an auditory cortical area known to send error signals to VTA (4/11 hemispheres; Figures S6I–S6K; Mandelblat-Cerf et al., 2014); (5)

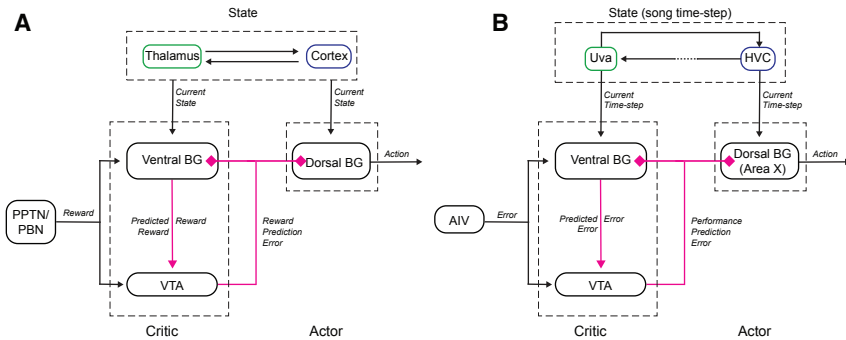
(G) A scatterplot of the mean firing rate during singing plotted against the ratio between mean firing rates during non-singing and singing periods identified VP neurons gated by singing state.

(H and I) Top to bottom: spectrograms, spiking activity, and corresponding instantaneous firing rate (IFR) for a song-on neuron, which fired at high rate during singing but was silent outside song (H), and a song-off neuron, which abruptly stopped firing during singing (I).

Scale bar for spiking activity in (B)–(F), (H), and (I) is 0.15 mV. See also Figure S3.



(legend on next page)



ovoidalis, the primary auditory thalamus (2/11 hemispheres; Figures S6M, S6N, and S6P; [Lei and Mooney, 2010](#); [Vates et al., 1996](#)); and (6) VTA (9/21 hemispheres; Figures S6Q–S6S).

We note that using this retrograde viral tracing strategy, we only observed sparsely labeled cells in all identified input regions to VP ([Figure S9](#)). This may indicate sparse connections between input regions and VP, but it could also be due to sparse uptake by axon terminals and/or sparse viral expression ([STAR Methods](#)). Indeed, in all VP-injected, birds we observed sparse input from the main known input to VP, area X ([Gale et al., 2008](#)) (not shown). We additionally used dual-tracer strategies and further confirmed that anterogradely labeled RA axons co-mingled with VTA-projecting VP neurons ($n = 1/2$ hemispheres; [Figures S6C and S6D](#)), retrograde tracers in VP and Area X colabeled AIV neurons (3/5 cells co-labeled in 3/3 hemispheres; [Figures S6I–S6L](#)), retrograde tracers in VP and Area X co-labeled VTA neurons ($n = 4/6$ cells co-labeled in 2/2 hemispheres; [Figures S6Q–S6T](#)), and retrograde tracers in VP and HVC co-labeled Uva neurons (3/9 cells co-labeled in 2/3 hemispheres; [Figures S6E–S6H](#)). Together, these data show that VP receives inputs from RA, DLM, ovoidalis, HVC-projecting Uva neurons, VTA_X neurons, and VTA-projecting AIV neurons.

DISCUSSION

By combining lesions, viral tracing, and electrophysiology, we discovered that songbird VP is required for song learning, receives information about song-syllable timing and error, and sends diverse performance prediction- and error-related signals to VTA. These findings demonstrate that VP circuits can play an essential role in performance evaluation during a purely motor sequence learning task like birdsong.

Despite the importance of error signals for motor sequence learning, the identification of online error signals remained elusive in singing birds ([Achiro et al., 2017](#); [Derégnaucourt et al., 2004](#); [Hahnloser and Ganguli, 2013](#)). HVC and LMAN do not exhibit re-

Figure 6. An Actor-Critic Circuit Motif for Computing Performance Prediction Error

(A) Actor-critic circuit motif in mammalian BG (adapted from [Daw et al., 2006](#); [Joel et al., 2002](#); [Takahashi et al., 2008](#)).

(B) Anatomy and signaling in songbird VP reveal a similar motif.

See also [Figure S6](#).

sponses to DAF during singing ([Hamaguchi et al., 2014](#); [Kozhevnikov and Fee, 2007](#); [Leonardo, 2004](#); [Vallentin and Long, 2015](#)), ruling against hypothesized roles of the classic song system in online evaluation of auditory feedback ([Doupe and Konishi, 1991](#); [Nottebohm et al., 1990](#); [Troyer and Doupe, 2000](#)). Recent studies instead support the idea that auditory cortical areas extract error signals and send them to VTA, which in turn sends dopaminergic prediction error signals to area X ([Fee and Goldberg, 2011](#); [Woolley, 2019](#)). Specifically, early stages of the auditory cortical hierarchy exhibit singing-related auditory responses that include DAF-driven modulations ([Keller and Hahnloser, 2009](#)), and AIV, a higher-order auditory cortical region, contains VTA-projecting neurons that are not simply activated by singing and instead are specifically activated by DAF-induced errors ([Mandelblat-Cerf et al., 2014](#)). VTA then sends performance error signals to area X that can modify future performance ([Gadagkar et al., 2016](#); [Hisey et al., 2018](#); [Xiao et al., 2018](#)). Our finding that both AIV and VP can modulate VTA_X firing supports the idea that song evaluation signals can reach the classic song system through the VTA projection to area X ([Gale and Perkel, 2010](#)).

VP is classically viewed as an output of the limbic system involved in seeking primary reinforcers such as food, drugs, or courtship ([McAlonan et al., 1993](#); [Mogenson et al., 1980](#); [Smith et al., 2009](#)). VP lesions in mammals cause anhedonia, reduce drug and food seeking, and impair reward-based place preference, implicating VP with both motivational “wanting” and hedonic “liking.” Consistent with this idea, VP neuronal activity is modulated by reward omissions, rewards, the cues that predict them, and their hedonic value ([Ahrens et al., 2016](#); [Ito and Doya, 2009](#); [Ottenheimer et al., 2018](#); [Richard et al., 2016, 2018](#); [Tachibana and Hikosaka, 2012](#); [Tindell et al., 2004](#)).

Computational models of basal ganglia (BG)-dependent RL may provide insight into how VP’s established hedonic functions relate to performance evaluation in singing birds. In classic actor-critic (AC) models, the BG has two functional subdivisions: a ventral “critic” with outputs to VTA and a dorsal “actor” with outputs to the motor system ([Figure 6A](#); [Daw et al., 2006](#); [Joel et al., 2002](#); [Takahashi et al., 2008](#)). Both subdivisions receive dopaminergic reward prediction error signals and implement

Figure 5. The VP Sends Diverse Error- and Prediction-Related Signals to the VTA

(A) Stimulation and recording electrodes were chronically implanted into VTA and VP, respectively, for antidromic identification of VTA-projecting VP neurons (VP_{VTA}).

(B) Antidromic (black) and collision (red) testing of the neuron shown in (C). Scale bars, 1 ms (horizontal) and 0.1 mV (vertical).

(C–K) Song-locked firing patterns of 9 VP_{VTA} neurons, plotted as in [Figure 3B](#), reveal diverse responses, including prediction errors with significant burst (C) or pause (D) at undistorted target time, pre-target burst (E), error-induced activation (F–H), and pre-target pauses (I–J). The y scale bar for spiking activity is 0.15 mV. See also [Figure S3](#).

DA-modulated plasticity to weigh cortical inputs (which encode “state”; **Figure 6A**) according to their reward value. DA modulated plasticity in the critic therefore computes predicted state value, for example a cue-dependent reward prediction. Predicted state-value coding by VP, manifest as VP responses to conditioned stimuli in Pavlovian tasks (Ahrens et al., 2016; Ito and Doya, 2009; Richard et al., 2018; Tindell et al., 2004), can provide VTA with “prediction” information necessary to compute reward prediction error (Tian et al., 2016). DA prediction error signals project back to the critic (to update predicted state-value) and also to an “actor.” The actor also implements DA-modulated plasticity on “state”-encoding inputs. Because the actor has topographically organized outputs to the motor system, this plasticity links a state representation to a reward-maximizing action (Daw et al., 2006; Joel et al., 2002; Takahashi et al., 2008), manifest as action-value coding in dorsal BG structures (Samejima and Doya, 2007).

Our findings suggest that songbird VP may implement some functions analogous to the critic in the classic AC architecture, including the computation of predicted state value (which in bird-song is analogous to predicted syllable quality). Specifically, thalamic (uva) or cortical (RA) inputs to VP could provide state representations in the form of “time step” in song that could explain the observed VP timing responses (**Figures 4B** and **4C**; Danish et al., 2017; Hamaguchi et al., 2016; Leonardo and Fee, 2005; Sober et al., 2008; Yu and Margoliash, 1996). Next, DA inputs to VP from VTA_X neurons could enable DA-modulated plasticity to weigh uva inputs according to past error. For example, consider a three-syllable song *a-b-c*. If syllable *b* is reliably distorted, then DA pauses (driven by AIV) would be coincident with those uva inputs active at syllable *b*. Then, DA-modulated plasticity of uva inputs would reweigh these synapses, resulting in a representation in VP of error-weighted timing or, equivalently, predicted error (**Figure 6B**). With an eligibility trace (Sutton and Barto, 1998; Yagishita et al., 2014), this process would explain the pre-target pauses observed in VP that are enriched in VP_{VTA} neurons (**Figures 5F–5K**). Finally, AIV neurons are DAF responsive during singing and could explain error responses in VP (**Figure 3**; Mandelblat-Cerf et al., 2014). Altogether, VP thus contains information necessary to signal the difference between predicted and actual error, manifest in the observed prediction error responses (**Figures 3A** and **3B**) that can be sent to VTA (**Figures 5C** and **5D**). A key prediction of this model is the existence of DA-modulated plasticity of uva or RA inputs to VP.

In biologically inspired AC models, the DA error signal reaches both ventral and dorsal BG domains (Daw et al., 2006; Joel et al., 2002; Takahashi et al., 2008). Notably, VP-projecting VTA neurons also project to area X, which is located more dorsolaterally and has topographically organized outputs to the song motor system (Johnson et al., 1995; Luo et al., 2001). DA-modulated plasticity in area X (Ding and Perkel, 2004) reinforces the way a target syllable is produced (Hisey et al., 2018; Hoffmann et al., 2016; Xiao et al., 2018), much like manipulation of striatal DA in mammals can reinforce place preference or action selection (Tsai et al., 2009; Wise and Schwartz, 1981). Thus, we propose that area X has anatomical and functional similarities to the actor in classic AC architecture (Charlesworth et al., 2012; Fee and Goldberg, 2011; **Figure 6B**), forming the counterpart to the ventral critic.

The AC model helps unify mechanisms of reward seeking and performance evaluation into a common framework, but it fails to explain the diversity of VP signals and likely oversimplifies processes underlying the construction of the dopaminergic error signal. First, VP stimulation could cause either activation or suppression of VTA_X firing (**Figures 1E**, **1F**, and **S2N–S2R**), which could be due to a mixture of glutamatergic and GABAergic VP_{VTA} neurons and/or differential engagement with local inhibition in VTA that can invert afferent signals (Yang et al., 2018). Second, VP_{VTA} neurons could be activated by distorted renditions, activated or suppressed by undistorted renditions, and exhibit pre-target bursts or pauses that may encode predicted song error or predicted quality, respectively (**Figure 5**). Thus VP sends virtually every conceivable error-related signal to VTA. While it is possible to linearly combine these VP signals in specific ways to construct the known VTA_X signal, it remains unclear how these mixed inputs are transformed by the VTA microcircuit into a remarkably homogeneous dopaminergic prediction error signal in the VTA_X pathway. Notably, mixed responses to reward and reward-predicting cues are observed in VP (and other) inputs to mammalian VTA, even though VTA output is a similarly homogeneous reward prediction error signal (Hong and Hikosaka, 2014; Tian et al., 2016). How relatively homogeneous DA error signals are constructed from mixed inputs is similarly elusive in birds and mammals and may involve complex, cell-type-specific engagement with VTA microcircuitry (Yang et al., 2018). Future recordings of VTA_X neurons in lesioned animals could clarify how DA pauses and bursts depend on specifically on inputs from AIV and VP (Takahashi et al., 2016; Takahashi et al., 2011; Tian and Uchida, 2015).

In summary, we report that the VP, a limbic structure associated with reward seeking in mammals, is necessary for birdsong learning, receives information from VTA and auditory and vocal motor areas, and sends diverse performance and prediction error signals to VTA.

STAR★METHODS

Detailed methods are provided in the online version of this paper and include the following:

- **KEY RESOURCES TABLE**
- **CONTACT FOR REAGENTS AND RESOURCE SHARING**
- **EXPERIMENTAL MODEL AND SUBJECT DETAILS**
 - Subjects
- **METHOD DETAILS**
 - Surgery and histology
 - Recording VTA responses to stimulation of AIV/VP
 - Song imitation score
 - Syllable-targeted distorted auditory feedback
 - Passive playback of the bird’s own song
 - Analysis of neural activity
 - Performance error response
 - Song timing related activity
- **QUANTIFICATION AND STATISTICAL ANALYSIS**
 - Quantification of movement
 - Imaging

SUPPLEMENTAL INFORMATION

Supplemental Information can be found online at <https://doi.org/10.1016/j.neuron.2019.04.038>.

A video abstract is available at <https://doi.org/10.1016/j.neuron.2019.04.038#mmc3>.

ACKNOWLEDGMENTS

We thank Todd Roberts for providing virus; Joe Fethcho, Teja Bollu, and Josh Dudman for comments; and Vikram Gadagkar, Aaron Andelman, and Dmitriy Aronov for comments and analysis code. Funding to J.H.G. was provided by the NIH (R01NS094667), the Pew Charitable Trust, and the Klingenstein Neuroscience Foundations. Funding to P.A.P. was provided by the NIH (F32NS098634). Imaging data were acquired in the Cornell BRC-Imaging Facility using the shared, NIH-funded (S10RR025502) Zeiss LSM 710 Confocal.

AUTHOR CONTRIBUTIONS

R.C., P.A.P., A.C.R., T.E.R., K.M., A.P., A.R.F., and J.H.G. acquired data. R.C., P.A.P., A.P., K.M., and J.H.G. analyzed data. R.C. and J.H.G. wrote the manuscript.

DECLARATION OF INTERESTS

The authors declare no competing interests.

Received: July 30, 2018

Revised: January 30, 2019

Accepted: April 25, 2019

Published: May 29, 2019

REFERENCES

- Achiro, J.M., Shen, J., and Bottjer, S.W. (2017). Neural activity in cortico-basal ganglia circuits of juvenile songbirds encodes performance during goal-directed learning. *eLife* 6, e26973.
- Ahrens, A.M., Meyer, P.J., Ferguson, L.M., Robinson, T.E., and Aldridge, J.W. (2016). Neural activity in the ventral pallidum encodes variation in the incentive value of a reward cue. *J. Neurosci.* 36, 7957–7970.
- Ali, F., Otczy, T.M., Pehlevan, C., Fantana, A.L., Burak, Y., and Ölveczky, B.P. (2013). The basal ganglia is necessary for learning spectral, but not temporal, features of birdsong. *Neuron* 80, 494–506.
- Andelman, A.S., and Fee, M.S. (2009). A basal ganglia-forebrain circuit in the songbird biases motor output to avoid vocal errors. *Proc. Natl. Acad. Sci. USA* 106, 12518–12523.
- Beier, K.T., Steinberg, E.E., DeLoach, K.E., Xie, S., Miyamichi, K., Schwarz, L., Gao, X.J., Kremer, E.J., Malenka, R.C., and Luo, L. (2015). Circuit architecture of VTA dopamine neurons revealed by systematic input-output mapping. *Cell* 162, 622–634.
- Bottjer, S.W., Brady, J.D., and Cribbs, B. (2000). Connections of a motor cortical region in zebra finches: relation to pathways for vocal learning. *J. Comp. Neurol.* 420, 244–260.
- Carr, D.B., and Sesack, S.R. (1999). Terminals from the rat prefrontal cortex synapse on mesoaccumbens VTA neurons. *Ann. N.Y. Acad. Sci.* 877, 676–678.
- Charlesworth, J.D., Warren, T.L., and Brainard, M.S. (2012). Covert skill learning in a cortical-basal ganglia circuit. *Nature* 486, 251–255.
- Creed, M.C., Ntamatyi, N.R., and Tan, K.R. (2014). VTA GABA neurons modulate specific learning behaviors through the control of dopamine and cholinergic systems. *Front. Behav. Neurosci.* 8, 8.
- Danish, H.H., Aronov, D., and Fee, M.S. (2017). Rhythmic syllable-related activity in a songbird motor thalamic nucleus necessary for learned vocalizations. *PLoS ONE* 12, e0169568.
- Daw, N.D., Niv, Y., and Dayan, P. (2006). Actions, policies, values and the basal ganglia. In *Recent Breakthroughs in Basal Ganglia Research*, E. Bezard, ed. (Nova Science Publishers), pp. 91–96.
- Derégnaucourt, S., Mitra, P.P., Fehér, O., Maul, K.K., Lints, T.J., and Tchernichovski, O. (2004). Song development: in search of the error-signal. *Ann. N.Y. Acad. Sci.* 1016, 364–376.
- Ding, L., and Perkel, D.J. (2004). Long-term potentiation in an avian basal ganglia nucleus essential for vocal learning. *J. Neurosci.* 24, 488–494.
- Doupe, A.J., and Konishi, M. (1991). Song-selective auditory circuits in the vocal control system of the zebra finch. *Proc. Natl. Acad. Sci. USA* 88, 11339–11343.
- Fee, M.S., and Goldberg, J.H. (2011). A hypothesis for basal ganglia-dependent reinforcement learning in the songbird. *Neuroscience* 198, 152–170.
- Gadagkar, V., Puzerey, P.A., Chen, R., Baird-Daniel, E., Farhang, A.R., and Goldberg, J.H. (2016). Dopamine neurons encode performance error in singing birds. *Science* 354, 1278–1282.
- Gale, S.D., and Perkel, D.J. (2010). A basal ganglia pathway drives selective auditory responses in songbird dopaminergic neurons via disinhibition. *J. Neurosci.* 30, 1027–1037.
- Gale, S.D., Person, A.L., and Perkel, D.J. (2008). A novel basal ganglia pathway forms a loop linking a vocal learning circuit with its dopaminergic input. *J. Comp. Neurol.* 508, 824–839.
- Hahnloser, R., and Ganguli, S. (2013). Vocal learning with inverse models. In *Principles of Neural Coding*, S. Panzeri and P. Quiroga, eds. (CRC Taylor and Francis), pp. 547–564.
- Goldberg, J.H., and Fee, M.S. (2010). Singing-related neural activity distinguishes four classes of putative striatal neurons in the songbird basal ganglia. *J. Neurophysiol.* 103, 2002–2014.
- Goldberg, J.H., and Fee, M.S. (2012). A cortical motor nucleus drives the basal ganglia-recipient thalamus in singing birds. *Nat. Neurosci.* 15, 620–627.
- Goldberg, J.H., Adler, A., Bergman, H., and Fee, M.S. (2010). Singing-related neural activity distinguishes two putative pallidal cell types in the songbird basal ganglia: comparison to the primate internal and external pallidal segments. *J. Neurosci.* 30, 7088–7098.
- Hamaguchi, K., Tschida, K.A., Yoon, I., Donald, B.R., and Mooney, R. (2014). Auditory synapses to song premotor neurons are gated off during vocalization in zebra finches. *eLife* 3, e01833.
- Hamaguchi, K., Tanaka, M., and Mooney, R. (2016). A distributed recurrent network contributes to temporally precise vocalizations. *Neuron* 91, 680–693.
- Hisey, E., Kearney, M.G., and Mooney, R. (2018). A common neural circuit mechanism for internally guided and externally reinforced forms of motor learning. *Nat. Neurosci.* 21, 589–597.
- Hoffmann, L.A., Saravanan, V., Wood, A.N., He, L., and Sober, S.J. (2016). Dopaminergic contributions to vocal learning. *J. Neurosci.* 36, 2176–2189.
- Hong, S., and Hikosaka, O. (2014). Pedunculopontine tegmental nucleus neurons provide reward, sensorimotor, and alerting signals to midbrain dopamine neurons. *Neuroscience* 282, 139–155.
- Ito, M., and Doya, K. (2009). Validation of decision-making models and analysis of decision variables in the rat basal ganglia. *J. Neurosci.* 29, 9861–9874.
- Joel, D., Niv, Y., and Ruppin, E. (2002). Actor-critic models of the basal ganglia: new anatomical and computational perspectives. *Neural Netw.* 15, 535–547.
- Johnson, F., Sablan, M.M., and Bottjer, S.W. (1995). Topographic organization of a forebrain pathway involved with vocal learning in zebra finches. *J. Comp. Neurol.* 358, 260–278.
- Kao, M.H., Wright, B.D., and Doupe, A.J. (2008). Neurons in a forebrain nucleus required for vocal plasticity rapidly switch between precise firing and variable bursting depending on social context. *J. Neurosci.* 28, 13232–13247.
- Keller, G.B., and Hahnloser, R.H. (2009). Neural processing of auditory feedback during vocal practice in a songbird. *Nature* 457, 187–190.
- Kelley, D.B., and Nottebohm, F. (1979). Projections of a telencephalic auditory nucleus-field L-in the canary. *J. Comp. Neurol.* 183, 455–469.

- Kozhevnikov, A.A., and Fee, M.S. (2007). Singing-related activity of identified HVC neurons in the zebra finch. *J. Neurophysiol.* 97, 4271–4283.
- Lei, H., and Mooney, R. (2010). Manipulation of a central auditory representation shapes learned vocal output. *Neuron* 65, 122–134.
- Leonardo, A. (2004). Experimental test of the birdsong error-correction model. *Proc. Natl. Acad. Sci. USA* 101, 16935–16940.
- Leonardo, A., and Fee, M.S. (2005). Ensemble coding of vocal control in birdsong. *J. Neurosci.* 25, 652–661.
- Luo, M., Ding, L., and Perkel, D.J. (2001). An avian basal ganglia pathway essential for vocal learning forms a closed topographic loop. *J. Neurosci.* 21, 6836–6845.
- Mandelblat-Cerf, Y., and Fee, M.S. (2014). An automated procedure for evaluating song imitation. *PLoS ONE* 9, e96484.
- Mandelblat-Cerf, Y., Las, L., Denisenko, N., and Fee, M.S. (2014). A role for descending auditory cortical projections in songbird vocal learning. *eLife* 3, e02152.
- Marler, P. (1997). Three models of song learning: evidence from behavior. *J. Neurobiol.* 33, 501–516.
- McAlonan, G.M., Robbins, T.W., and Everitt, B.J. (1993). Effects of medial dorsal thalamic and ventral pallidal lesions on the acquisition of a conditioned place preference: further evidence for the involvement of the ventral striatopallidal system in reward-related processes. *Neuroscience* 52, 605–620.
- Mello, C.V., Vates, G.E., Okuhata, S., and Nottebohm, F. (1998). Descending auditory pathways in the adult male zebra finch (*Taeniopygia guttata*). *J. Comp. Neurol.* 395, 137–160.
- Mogenson, G.J., Jones, D.L., and Yim, C.Y. (1980). From motivation to action: functional interface between the limbic system and the motor system. *Prog. Neurobiol.* 14, 69–97.
- Moreines, J.L., Owrtusky, Z.L., and Grace, A.A. (2017). Involvement of infralimbic prefrontal cortex but not lateral habenula in dopamine attenuation after chronic mild stress. *Neuropsychopharmacology* 42, 904–913.
- Murdoch, D., Chen, R., and Goldberg, J.H. (2018). Place preference and vocal learning rely on distinct reinforcers in songbirds. *Sci. Rep.* 8, 6766.
- Nottebohm, F., Alvarez-Buylla, A., Cynx, J., Kim, J., Ling, C.Y., Nottebohm, M., Suter, R., Tolles, A., and Williams, H. (1990). Song learning in birds: the relation between perception and production. *Philos. Trans. R. Soc. Lond. B Biol. Sci.* 329, 115–124.
- Olveczky, B.P., Andelman, A.S., and Fee, M.S. (2005). Vocal experimentation in the juvenile songbird requires a basal ganglia circuit. *PLoS Biol.* 3, e153.
- Ottenheimer, D., Richard, J.M., and Janak, P.H. (2018). Ventral pallidum encodes relative reward value earlier and more robustly than nucleus accumbens. *Nat. Commun.* 9, 4350.
- Patton, M.H., Bizup, B.T., and Grace, A.A. (2013). The infralimbic cortex bidirectionally modulates mesolimbic dopamine neuron activity via distinct neural pathways. *J. Neurosci.* 33, 16865–16873.
- Person, A.L., Gale, S.D., Farries, M.A., and Perkel, D.J. (2008). Organization of the songbird basal ganglia, including area X. *J. Comp. Neurol.* 508, 840–866.
- Reiner, A., Perkel, D.J., Mello, C.V., and Jarvis, E.D. (2004). Songbirds and the revised avian brain nomenclature. *Ann. N Y Acad. Sci.* 1016, 77–108.
- Richard, J.M., Ambroggi, F., Janak, P.H., and Fields, H.L. (2016). Ventral pallidum neurons encode incentive value and promote cue-elicited instrumental actions. *Neuron* 90, 1165–1173.
- Richard, J.M., Stout, N., Acs, D., and Janak, P.H. (2018). Ventral pallidal encoding of reward-seeking behavior depends on the underlying associative structure. *eLife* 7, e33107.
- Samejima, K., and Doya, K. (2007). Multiple representations of belief states and action values in corticobasal ganglia loops. *Ann. N Y Acad. Sci.* 1104, 213–228.
- Schmidt, R.A., Lee, T., Weinstein, C., Wulf, G., and Zelaznik, H. (2018). Motor Control and Learning, 6E (Human Kinetics).
- Schultz, W., and Romo, R. (1987). Responses of nigrostriatal dopamine neurons to high-intensity somatosensory stimulation in the anesthetized monkey. *J. Neurophysiol.* 57, 201–217.
- Smith, K.S., Tindell, A.J., Aldridge, J.W., and Berridge, K.C. (2009). Ventral pallidum roles in reward and motivation. *Behav. Brain Res.* 196, 155–167.
- Sober, S.J., Wohlgemuth, M.J., and Brainard, M.S. (2008). Central contributions to acoustic variation in birdsong. *J. Neurosci.* 28, 10370–10379.
- Sutton, R.S., and Barto, A.G. (1998). Reinforcement Learning: an Introduction (MIT Press).
- Tachibana, Y., and Hikosaka, O. (2012). The primate ventral pallidum encodes expected reward value and regulates motor action. *Neuron* 76, 826–837.
- Takahashi, Y., Schoenbaum, G., and Niv, Y. (2008). Silencing the critics: understanding the effects of cocaine sensitization on dorsolateral and ventral striatum in the context of an actor/critic model. *Front. Neurosci.* 2, 86–99.
- Takahashi, Y.K., Roesch, M.R., Wilson, R.C., Toreson, K., O'Donnell, P., Niv, Y., and Schoenbaum, G. (2011). Expectancy-related changes in firing of dopamine neurons depend on orbitofrontal cortex. *Nat. Neurosci.* 14, 1590–1597.
- Takahashi, Y.K., Langdon, A.J., Niv, Y., and Schoenbaum, G. (2016). Temporal specificity of reward prediction errors signaled by putative dopamine neurons in rat VTA depends on ventral striatum. *Neuron* 97, 182–193.
- Tchernichovski, O., Nottebohm, F., Ho, C.E., Pesaran, B., and Mitra, P.P. (2000). A procedure for an automated measurement of song similarity. *Anim. Behav.* 59, 1167–1176.
- Thelen, E. (1995). Motor development. A new synthesis. *Am. Psychol.* 50, 79–95.
- Tian, J., and Uchida, N. (2015). Habenula lesions reveal that multiple mechanisms underlie dopamine prediction errors. *Neuron* 87, 1304–1316.
- Tian, J., Huang, R., Cohen, J.Y., Osakada, F., Kobak, D., Machens, C.K., Callaway, E.M., Uchida, N., and Watabe-Uchida, M. (2016). Distributed and mixed information in monosynaptic inputs to dopamine neurons. *Neuron* 91, 1374–1389.
- Tindell, A.J., Berridge, K.C., and Aldridge, J.W. (2004). Ventral pallidal representation of Pavlovian cues and reward: population and rate codes. *J. Neurosci.* 24, 1058–1069.
- Troyer, T.W., and Doupe, A.J. (2000). An associational model of birdsong sensorimotor learning I. Efference copy and the learning of song syllables. *J. Neurophysiol.* 84, 1204–1223.
- Tsai, H.C., Zhang, F., Adamantidis, A., Stuber, G.D., Bonci, A., de Lecea, L., and Deisseroth, K. (2009). Phasic firing in dopaminergic neurons is sufficient for behavioral conditioning. *Science* 324, 1080–1084.
- Tumer, E.C., and Brainard, M.S. (2007). Performance variability enables adaptive plasticity of 'crystallized' adult birdsong. *Nature* 450, 1240–1244.
- Vallentin, D., and Long, M.A. (2015). Motor origin of precise synaptic inputs onto forebrain neurons driving a skilled behavior. *J. Neurosci.* 35, 299–307.
- Vates, G.E., Broome, B.M., Mello, C.V., and Nottebohm, F. (1996). Auditory pathways of caudal telencephalon and their relation to the song system of adult male zebra finches. *J. Comp. Neurol.* 366, 613–642.
- Wise, R.A., and Schwartz, H.V. (1981). Pimozide attenuates acquisition of lever-pressing for food in rats. *Pharmacol. Biochem. Behav.* 15, 655–656.
- Woolley, S.C. (2019). Dopaminergic regulation of vocal-motor plasticity and performance. *Curr. Opin. Neurobiol.* 54, 127–133.
- Woolley, S.C., Rajan, R., Joshua, M., and Doupe, A.J. (2014). Emergence of context-dependent variability across a basal ganglia network. *Neuron* 82, 208–223.
- Xiao, L., Chattree, G., Oscos, F.G., Cao, M., Wanat, M.J., and Roberts, T.F. (2018). A basal ganglia circuit sufficient to guide birdsong learning. *Neuron* 98, 208–221.e205.
- Yagishita, S., Hayashi-Takagi, A., Ellis-Davies, G.C., Urakubo, H., Ishii, S., and Kasai, H. (2014). A critical time window for dopamine actions on the structural plasticity of dendritic spines. *Science* 345, 1616–1620.
- Yang, H., de Jong, J.W., Tak, Y., Peck, J., Bateup, H.S., and Lammel, S. (2018). Nucleus accumbens subnuclei regulate motivated behavior via direct inhibition and disinhibition of VTA dopamine subpopulations. *Neuron* 97, 434–449.e434.
- Yu, A.C., and Margoliash, D. (1996). Temporal hierarchical control of singing in birds. *Science* 273, 1871–1875.

STAR★METHODS

KEY RESOURCES TABLE

REAGENT or RESOURCE	SOURCE	IDENTIFIER
Antibodies		
Anti-Tyrosine Hydroxylase antibody	Millipore	Cat#AB152
Anti-NeuN antibody, Alexa Fluor 488 conjugated	Millipore	Cat#MAB377Xclone A60
Bacterial and Virus Strains		
Self-complementary AAV9-CBh-GFP	Gene Therapy Center Vector Core, University of North Carolina at Chapel Hill	N/A
Short Term HSV-mCherry	Gene Delivery Technology Core, Massachusetts General Hospital	Cat#RN3
Chemicals, Peptides, and Recombinant Proteins		
N-Methyl-DL-aspartic acid	Sigma	Cat#M2137
Experimental Models: Organisms/Strains		
Zebra Finch (<i>Taeniopygia guttata</i>)	Magnolia Bird Farm, Anaheim CA	N/A
Software and Algorithms		
MATLAB	MathWorks	https://www.mathworks.com/products/matlab.html
ImageJ	NIH	https://imagej.nih.gov/ij/
Sound Analysis Pro	Tchernichovski et al., 2000	N/A
Similarity Index	Mandelblat-Cerf and Fee, 2014	N/A

CONTACT FOR REAGENTS AND RESOURCE SHARING

Further information and requests for resources and reagents should be directed to and will be fulfilled by the Lead Contact, Jesse H. Goldberg (jessehgoldberg@gmail.com).

EXPERIMENTAL MODEL AND SUBJECT DETAILS

Subjects

Subjects were 91 male zebra finches (at least 39 days post hatch, dph). Animal care and experiments were carried out in accordance with NIH guidelines and were approved by the Cornell Institutional Animal Care and Use Committee.

METHOD DETAILS

Surgery and histology

All surgeries were performed with isoflurane anesthetization. For functional mapping experiments (8 birds, 90 dph or older, Figure. 1), bipolar stimulation electrodes were implanted into AIY and Area X ([Gadagkar et al., 2016](#); [Mandelblat-Cerf et al., 2014](#)). In 4/8 birds, additional stimulation electrodes were implanted into VP. AIY coordinate was determined by its anterior and ventral position to RA, and Area X coordinate was +5.6A, +1.5L relative to lambda and 2.65 ventral relative to pial surface, at a head angle of 20 degrees. VP coordinate was +4.9A, +1.3L relative to lambda and 3.9 ventral to pial surface at a head angle of 20 degrees. Recordings were made in VTA using a carbon fiber electrode (1 MOhm, Kation Scientific). VTA was identified by anatomical landmarks. Specifically, the boundaries of DLM and Ovoidalis were determined by spontaneous firing and auditory responses. Recordings were then made at the same AP position, +0.6L relative to lambda and 6.5 ventral relative to pial surface, at a head angle of 55 degrees. This AP position corresponds to the anterior part of VTA enriched in Area X projecting neurons (VTA_X) ([Gadagkar et al., 2016](#); [Mandelblat-Cerf et al., 2014](#)). VTA_X neurons were further confirmed by antidromic response and collision testing. At the end of the experiment, small electrolytic lesions (30 uA for 60 s) were made at each stimulation site. Location of the stimulating electrodes was verified histologically.

For VP lesion (13 birds, 39-52 dph), a bipolar stimulation electrode was implanted into Area X and the boundaries of VP was electrophysiologically mapped by finding units suppressed by Area X stimulation. 115nl of 2% N-methyl-DLaspartic acid (NMA; Sigma, St Louis, MO) or saline (for control birds) was injected into VP bilaterally. Lesions were histologically confirmed by labeling neurons with anti-NeuN (full bilateral VP lesions in 6 birds).

For awake-behaving electrophysiology (39 birds, 87–355 dph), custom made microdrives carrying an accelerometer (Analog Devices AD22301), linear actuator (Faulhaber 0206 series micromotor) and homemade electrode arrays (5 electrodes, 3–5 MΩms, microprobe.com) were implanted into VP by coordinates (4.4–5.4A, 1.1–1.5L, 3.5V, head angle 20 degrees). In 20/39 birds, a bipolar stimulation electrode was implanted into VTA using anatomical landmarks as described above. After each experiment, small electrolytic lesions (30 μA for 60 s) were made with one of the recording electrodes. Brains were then fixed, cut into 100 μm thick sagittal sections for histological confirmation of stimulation electrode tracks and reference lesions.

For VP tracing experiments (31 birds, 90 dph or older), 40nl of self-complementary adeno-associated virus carrying green fluorescent protein (scAAV9-CBh-GFP, UNC vector core) was injected into VP in two coordinates (4.6/4.9A, 1.3L, 4V). Upstream neurons retrogradely infected and expressing GFP could be observed in RA, AIV, Uva, Ov, DLM, and VTA (each input was checked in a subset of birds as indicated in the main text). To determine if VP shares common inputs with HVC, in addition to scAAV9 in VP, fluorescently labeled cholera toxin subunit B (CTB, Molecular Probes) was injected into HVC in 3 birds. To determine if VP share common inputs with Area X, CTB was injected into Area X for 2 birds. To test if RA axons co-mingle with VTA projecting VP neurons, CTB was injected into VTA and anterograde HSV-mCherry (MGH viral core) was injected into RA.

Recording VTA responses to stimulation of AIV/VP

Neurons were classified as Area X-projecting (VTA_X) based on antidromic stimulation and collision testing (200 μs pulses, 100–300 μA). Spike duration was determined by the interval between onset and offset time of spikes (Figures 1C and S2K). VTA neurons that did not respond to Area X stimulation were classified as putative interneurons. We cannot rule out the possibility that a subset of these neurons project to the basal ganglia outside the field of influence of stimulation. A burst of AIV (or VP) stimulation consisting three 200 μs pulses with 10ms inter-pulse-interval was delivered every 1.5–2 s, with 300 μA current amplitude. Putative interneurons were also tested for response to AIV stimulation. VTA_X neurons were found in an anterior part of VTA, intermingled with non-projecting local neurons (Gadagkar et al., 2016; Mandelblat-Cerf et al., 2014).

All VTA_X neurons and those putative interneurons with rate influenced by AIV stimulation were further analyzed. To determine if VTA neurons respond to AIV (VP) stimulation, spiking activity within ± 1 s relative to stimulation onset was binned in a moving window of 30ms (for VTA_X neurons) or 10ms (for VTA interneurons) with a step size of 5ms. Each bin after stimulation onset was tested against all the bins in the previous 1 s (the prior) using a Z test. Windows where at least 2 consecutive bins with $p < 0.05$ were considered significant. The response onset and offset were required to bracket lowest (for phasic decrease) or highest (for phasic increase) firing rate after stimulation onset. Response was quantified by normalized firing rate in the first significant window using the 1 s before stimulation onset as baseline (Figure S2L).

To determine if the simultaneously recorded putative interneuron (PIN) and VTA_X neuron were correlated, we constructed rate histogram of VTA_X neuron spiking events aligned to spontaneous spiking events of PIN with preceding inter-spike interval (ISI) > 10ms, and assessed significance of rate changes of VTA_X neuron using Z test (Figure 1D).

Song imitation score

Song learning in VP lesioned and control birds was assessed by song similarity between pupil (at 90 dph) and their tutors. We computed imitation scores using an automated procedure based on Sound Analysis Pro (SAP) algorithm (Mandelblat-Cerf and Fee, 2014; Tchernichovski et al., 2000). Briefly, the tutor motif was segmented into syllables by hand. Syllables in the pupil song were determined by finding the section of pupil song with highest SAP similarity to each tutor syllable. Additionally, a sequencing score was computed as the similarity of the next syllable in tutor song and the next section in the pupil song. Imitation score was the product of song similarity and sequence similarity (Mandelblat-Cerf et al., 2014).

Syllable-targeted distorted auditory feedback

Postoperative birds with microdrive implant were placed in a sound isolation chamber and given at least a day to habituate to distorted auditory feedback (DAF) as described previously (Gadagkar et al., 2016). Briefly, ongoing singing was analyzed by Labview software to target specific syllables, and two speakers inside the chamber played a 50ms DAF sound on top of bird's singing on 50% of randomly selected target renditions. DAF was either a broadband sound band passed at 1.5–8 kHz, the same spectral range of zebra finch song, or a segment of one of the bird's own non-target syllables displaced in time.

Passive playback of the bird's own song

For passive playback of the bird's own song (BOS), we played back randomly interleaved renditions of the undistorted and distorted motifs of the bird's own song during awake, non-singing periods. The loudness of playback was adjusted to match the average peak loudness of zebra finch song (Gadagkar et al., 2016; Mandelblat-Cerf et al., 2014).

Analysis of neural activity

Neural signals were band-passed filtered (0.25–15 kHz) in homemade analog circuits and acquired at 40 kHz using custom MATLAB software. Single units were identified as VTA-projecting by antidromic identification and antidromic collision testing (Figures 5A and 5B). Spike sorting was performed offline using custom MATLAB software. Instantaneous firing rates (IFR) were defined at each time point as the inverse of the enclosing ISI. Firing rate histograms were constructed with 10 ms bins and smoothed with a 3-bin moving

average, except for Figures 4C and 4D, where the histograms had 4ms and 5ms bins. All data were acquired during undirected song, except for the neuron in Figure 5K, which was recorded during female-directed song.

Performance error response

To identify performance-error related neurons, we assessed the difference in firing rate between distorted and undistorted singing renditions as previously described (Keller and Hahnloser, 2009; Mandelblat-Cerf et al., 2014). Neurons with less than 10 trials of either distorted or undistorted renditions of the target syllable were excluded from this analysis ($n = 34/162$ excluded). Briefly, we performed a WRS test on the number of spikes in distorted versus undistorted renditions in 30 ms windows. Windows were shifted in 5 ms steps and considered significant when at least 4 consecutive windows had $p < 0.05$. Error-related neurons were classified as error-activated if the firing rate is higher in distorted trials in window of significance, and error suppressed if the firing rate is higher in undistorted trials.

To visualize error response, we calculated z-score of the difference between distorted and undistorted rate histograms (Figure 3E). We defined ‘error score’ for each neuron to be the maximum of absolute z-scored difference in the 125ms after target onset (Figure 4A).

To identify prediction-error related neurons, we quantified phasic rate changes following undistorted target time. 1000 surrogate rate histograms were generated by randomly time-shifting each trial of undistorted target aligned data over the duration of the motif. Response was considered significant when firing rate dropped below 5th percentile or exceeded 95th percentile of the surrogate data. Neurons with significant rate peak or nadir in the window of significance for error response were identified as prediction error neurons.

To test if error responses were attributable to purely auditory responses to a different sound, we performed the same analysis for distorted and undistorted renditions during passive playback of bird’s own song (BOS) playback in 16/31 error neurons and 19/97 non-error neurons. Only two neurons exhibited an error response during passive playback. One such neuron exhibited similar song-locked firing during both singing and listening (Figure S5C). One other error responsive neuron also had song time-locked response in BOS playback, although the part of playback that contained target syllable was consistently masked by calls (Figure S5D).

We compared the latency and duration of error response to those of VTA_X neurons from a previous dataset (Gadagkar et al., 2016). Latency and duration were defined by the onset and onset-offset interval of significant windows in WRS test as described above.

To test if VP_{VTA} neurons were more likely to exhibit error response, we assigned a value of 1 (if error responsive) or 0 (if not error responsive) to each neuron tested for VTA antidromic stimulation. VP_{VTA} neurons were tested against the group of VP neurons tested but not antidromic using WRS test ($p = 0.05$).

Song timing related activity

Sparseness index was used to identify putative song-related MSNs. This distinguishes MSNs from other striatal cell types in the dorsal basal ganglia nucleus Area X (Goldberg and Fee, 2010). For each neuron, we calculated rate histograms aligned to syllable onset for all syllables. Then we normalized these histograms over all syllables to generate a probability density function p_i over N bins. An entropy-based sparseness index was computed as follows:

$$\text{Sparseness Index} = 1 + \frac{\sum_{i=1}^N p_i \log(p_i)}{\log(N)}$$

Intermotif pairwise correlation coefficient (IMCC) was used to identify neurons that had highly time-locked firing to song motifs (timing neurons), as previously described (Goldberg et al., 2010; Goldberg and Fee, 2010; Kao et al., 2008; Olveczky et al., 2005; Woolley et al., 2014). Motif aligned IFR was time warped to the median duration of all motifs, mean-subtracted, and smoothed with a Gaussian kernel of 20ms SD, resulting in \mathbf{r}_i for each motif. IMCC was defined as the mean value of all pairwise CC between \mathbf{r}_i as follows:

$$\text{IMCC} = \frac{1}{N_{\text{pairs}}} \sum_{j>i}^{N_{\text{pairs}}} \text{CC}_{ij}$$

$$\text{CC}_{ij} = \frac{\mathbf{r}_i \cdot \mathbf{r}_j}{\sqrt{\mathbf{r}_i^2 \mathbf{r}_j^2}}$$

To assess the significance of IMCC values, we computed new IMCC for each neuron by adding random, circular time shifts to each spiketrain. This was repeated 1000 times. IMCC was considered significant when the real value was greater than the 95th percentile of the shuffled data.

To quantify significant song-locked rate modulations, we compared the highest rate peak and lowest nadir in target-aligned rate histogram to 1000 surrogate rate histograms generated by randomly time-shifting spike trains. Rate peaks exceeding the 95th percentile of surrogate rate maximum and rate nadirs below the 5th percentile of surrogate rate minimum were considered significant.

To test if VPvta neurons were more likely to exhibit rate maxima/minima immediately prior to target time, we assigned a value of 1 (if a significant rate maximum/minimum was present in the 100ms before target time) or 0 (if significant peak/nadir was not present) for each neuron tested for VTA antidromic stimulation. VPvta neurons were tested against the group of VP neurons tested but not antidromic using WRS test ($p = 0.05$).

QUANTIFICATION AND STATISTICAL ANALYSIS

Quantification of movement

An accelerometer (Analog Devices AD22301) was mounted on microdrives to quantify gross body movements as described previously (Gadagkar et al., 2016). Briefly, movement onsets and offsets were determined by threshold crossings of the band-passed, rectified accelerometer signal. To test if error responses could be explained by a difference in movement rate following DAF, for each bird we calculated onset times of movements relative to song target time. Then we performed a WRS test ($p = 0.05$) on the number of movement onsets in distorted versus undistorted renditions in 30 ms windows. Windows were shifted in 5 ms steps and considered significant when at least 4 consecutive windows had $p < 0.05$.

Imaging

Imaging data were acquired with a Leica DM4000 B microscope and a Zeiss LSM 710 Confocal microscope. Image processing was done with ImageJ.